Mutational Analysis of cis-Acting RNA Signals in Segment 7 of Influenza A Virus

JOURNAL OF VIROLOGY, Dec. 2008, p. 11869–11879 Vol. 82, No. 23
0022-538X/08/$08.00+0 doi:10.1128/JVI.01634-08

Mutational Analysis of *cis*-Acting RNA Signals in Segment 7 of Influenza A Virus[▽]

Edward C. Hutchinson,[1] Martin D. Curran,[2] Eliot K. Read,[1] Julia R. Gog,[3] and Paul Digard[1]*

Division of Virology, Department of Pathology, University of Cambridge, Tennis Court Road, Cambridge CB2 1QP,[1] Health Protection Agency, Clinical Microbiology and Public Health Laboratory, Addenbrooke's Hospital, Hills Road, Cambridge CB2 2QW,[2] and DAMTP, Centre for Mathematical Sciences, University of Cambridge, Wilberforce Road, Cambridge CB3 0WA,[3] United Kingdom

Received 31 July 2008/Accepted 12 September 2008

The genomic viral RNA (vRNA) segments of influenza A virus contain specific packaging signals at their termini that overlap the coding regions. To further characterize *cis*-acting signals in segment 7, we introduced synonymous mutations into the terminal coding regions. Mutation of codons that are normally highly conserved reduced virus growth in embryonated eggs and MDCK cells between 10- and 1,000-fold compared to that of the wild-type virus, whereas similar alterations to nonconserved codons had little effect. In all cases, the growth-impaired viruses showed defects in virion assembly and genome packaging. In eggs, nearly normal numbers of virus particles that in aggregate contained apparently equimolar quantities of the eight segments were formed, but with about fourfold less overall vRNA content than wild-type virions, suggesting that, on average, fewer than eight segments per particle were packaged. Concomitantly, the particle/PFU and segment/PFU ratios of the mutant viruses showed relative increases of up to 300-fold, with the behavior of the most defective viruses approaching that predicted for random segment packaging. Fluorescent staining of infected cells for the nucleoprotein and specific vRNAs confirmed that most mutant virus particles did not contain a full genome complement. The specific infectivity of the mutant viruses produced by MDCK cells was also reduced, but in this system, the mutations also dramatically reduced virion production. Overall, we conclude that segment 7 plays a key role in the influenza A virus genome packaging process, since mutation of as few as 4 nucleotides can dramatically inhibit infectious virus production through disruption of vRNA packaging.

Influenza A virus is one of the world's major uncontrolled pathogens, causing seasonal epidemics as well as global pandemics (51). The negative-sense RNA of the influenza A virus genome is divided into eight segments, which has important genetic consequences for the virus. Notably, reassortment of segments from different viruses has created at least two pandemic strains within the last century (52), and genome segmentation may increase the stability of the genome by allowing the purging of miscopied segments (4, 33). However, segmentation also results in a packaging problem. Influenza virions do not typically package more than eight segments (18, 22, 37, 39, 53). Simplistically, incorporation of eight segments at random would result in a small minority of viruses (around 1 in 400, or $10^{-2.6}$) incorporating the complete genome (37), rendering the vast majority nonviable. Consequently, the virus has evolved a selective packaging mechanism which ensures that virions incorporate one copy of each of the genomic segments (13, 16). Packaging signals have now been defined through deletion mapping experiments, using reverse genetics and recombinant viral RNA (vRNA) molecules, for seven of the eight segments (11, 12, 15, 16, 23, 35, 41). Consistent with the structure of defective-interfering RNAs (21), these signals are generally located toward the termini of each vRNA segment, involving the noncoding regions but always extending some way into the coding region.

The means by which segment packaging signals operate is currently unclear. The favored hypothesis is that intersegment RNA-RNA interactions build up a specific complex containing one copy of each of the eight vRNAs (16, 36). This model is consistent with electron microscopy (EM) studies showing that virions tend to package eight ribonucleoproteins (RNPs) aligned along their long axes in an array of seven around one (18, 39, 53). However, prediction of putative interacting sequences is rendered difficult by the fact that vRNA molecules are encapsidated into a helical RNP structure (29, 38, 42, 54) and also by the possibility of non-Watson-Crick base pairing (17). Better delineation of the signals would be useful, but this is complicated by the overlap of *cis*-acting functions with open reading frames. To address this, we previously analyzed codon variability within the coding regions of influenza A virus and demonstrated that variation was highly restricted in areas of the genome known to have *cis*-acting functions, implying selection for the primary RNA sequence as well as for the encoded protein (17). This information was successfully used to predict individual functionally important nucleotides within the packaging signals of segments 1 and 6 of the virus (17, 27). Here we report the results of a further reverse genetic study in which codon variation was used to investigate *cis*-acting RNA functions in segment 7, the final vRNA for which no published experimental information on packaging signals is available. We show that synonymous changes to conserved codons, but not to nonconserved codons, within the predicted packaging signal of the segment drastically reduce virus fitness and produce a consistent phenotype of defective virus assembly whose mechanistic details indicate a key role for segment 7 in genome packaging.

* Corresponding author. Mailing address: Division of Virology, Department of Pathology, University of Cambridge, Tennis Court Road, Cambridge CB2 1QP, United Kingdom. Phone: 44 1223 336920. Fax: 44 1223 336926. E-mail: pd1@mole.bio.cam.ac.uk.

▽ Published ahead of print on 24 September 2008.

MATERIALS AND METHODS

Cells, virus, plasmids, and antisera. Human embryonic kidney 293T cells and Madin-Darby canine kidney (MDCK) cells were cultured as described previously (7). Influenza A/PR/8/34 (PR8) virus was generated using an eight-plasmid reverse genetic system kindly donated by R. Fouchier (8). Site-directed mutagenesis of the reverse genetic plasmids was carried out using mismatched PCR primers and native *Pfu* polymerase (Stratagene). Plasmids were sequenced using a combination of terminal primers and (where necessary) internal primers by the University of Cambridge Department of Biochemistry sequencing facility. Primers and PCR conditions are available on request. Plasmids pCDNA-PB1, pCDNA-NP, and pCDNA-M1 have been described previously (34, 40). Plasmid pCB8+, containing a cDNA copy of segment 8 from the Mt. Sinai strain of PR8 cloned into plasmid pSP65 (Promega), was obtained from S. Inglis. Rabbit anti-NP and anti-M1 sera have been described previously (2, 40), while the 14C2 anti-M2 monoclonal antibody was purchased from Abcam. Secondary antibodies were purchased from Molecular Probes or LiCor Biosciences (fluorescent conjugates) or from Dako (horseradish peroxidase conjugates).

Reverse genetics and virus titrations. To produce recombinant viruses, 10^6 293T cells were transfected with 1 μg of each plasmid and 10 μl Lipofectin in Opti-MEM (Gibco-BRL). After overnight incubation, the medium was changed to virus growth medium (Dulbecco's modified Eagle's medium supplemented with L-glutamine, penicillin, streptomycin, 1 μg/ml trypsin [Worthington Biochemical Corporation], and 0.14% bovine serum albumin), and the cells were incubated for 48 h. Virus-containing supernatant was then clarified by low-speed centrifugation (5 min at 1,000 × *g*). To produce working stocks of virus, 0.2 ml of each supernatant was used to infect confluent T75 flasks of MDCK cells, which were maintained for 48 h in 15 ml virus growth medium. Additional stocks were produced by inoculating either 100 or 1,000 PFU of virus, depending on the experiment, into the allantoic cavity of 8-day-old embryonated chicken eggs and incubating them at 37°C for 48 h. Segment 7 from all stocks of virus was sequenced to confirm the presence of the desired mutations. RNAs were extracted from infected cells by use of the SV Wizard total RNA isolation system (Promega) or from virus stocks by use of Tri Reagent LS (Sigma), reverse transcribed using avian myeloblastosis virus reverse transcriptase (Promega) and a terminal vRNA-binding primer, and amplified by PCR using terminal primers and Illustra *Taq* DNA polymerase (GE Healthcare).

Plaque assays were carried out on confluent MDCK cells as described previously (30). For plaque size analysis, toluidine blue-stained dishes were scanned, and ImageJ (1) was used to quantify areas of manually selected oval regions drawn around plaques. Hemagglutination (HA) assays were carried out in 96-well round-bottomed plates at room temperature, using 50 μl of virus dilution and 50 μl of a 1% suspension of chicken red blood cells in phosphate-buffered saline (PBS). To determine the infectious titers of stocks, cells were infected with serial dilutions of virus and stained by immunofluorescence for NP expression at 8 h postinfection (p.i.). The proportion of infected cells in a partially infected sample was used to calculate the multiplicity of infection, using the Poisson formula, and hence the titer of infectious virus. To determine virus particle number by EM, 10 μl of virus was diluted 1:1 with water containing 10^{10} 0.2-μm polystyrene latex spheres (TAAB Laboratories Equipment) and 3 μg bovine serum albumin. The mixture was adsorbed onto a glow-discharged 3-mm Formvar-carbon-coated gold grid (TAAB Laboratories Equipment), rinsed three times in water, and negatively stained with 2% phosphotungstic acid, pH 6.8. Grids were imaged with a Philips CM100 transmission electron microscope.

Microscopy. For immunofluorescence, MDCK cells grown on coverslips were processed as previously described (14). Fluorescence in situ hybridization (FISH) was performed essentially as previously described (2). To synthesize vRNA-binding probes, 4 μg of pCDNA-PB1, pCDNA-NP, pCDNA-M1, or pCB8+ was linearized (with EcoRI for pCDNA-M1 and XbaI for the others), and RNA was transcribed using T7 RNA polymerase (for pCDNA plasmids) or SP6 RNA polymerase (for pCB8+) in the presence of 0.25 mM cyanine 3-UTP or cyanine 5-UTP (Perkin-Elmer). Fluorescence images were captured using a Leica TCS-NT confocal microscope. To visualize particle budding, MDCK cells were processed as described previously (44) and then imaged with a Philips CM100 transmission electron microscope.

Protein and RNA analyses. Infected cell lysates were analyzed by sodium dodecyl sulfate-polyacrylamide gel electrophoresis (SDS-PAGE) and Western blotting according to standard procedures. Blots were imaged by chemiluminescence, using horseradish peroxidase-conjugated secondary antibodies and X-ray film, or by fluorescence (for quantification), using IRDye 800-conjugated secondary antibodies on a LiCor Biosciences Odyssey near-infrared imaging platform. To examine the protein content of virus particles, stocks were clarified by low-speed centrifugation, diluted to 0.8 ml in PBS, and pelleted through a 0.5-ml cushion of 33% sucrose in PBS, using a TLA55 rotor in a Beckman Optima Max-E benchtop ultracentrifuge at 91,000 × *g* for 45 min at 4°C; pellets were resuspended in 20 μl SDS-PAGE sample buffer. The vRNA content of infected cells was determined by reverse transcriptase primer extension analysis as previously described (34). Segment 7 mRNA species were detected by reverse transcription-PCR (RT-PCR) using an oligo(dT) primer for first-strand synthesis followed by PCR with a primer complementary to the 3′ ends of both mRNAs and either a primer complementary to the M2 intron (for M1 mRNA) or a primer spanning the 3′ intron-exon boundary (for M2 mRNA) (5). For analysis of the vRNA content of virus particles, 1.5-ml aliquots of clarified allantoic fluid were pelleted through a 3-ml cushion of 25% sucrose in NTE (100 mM NaCl, 10 mM Tris, pH 7.4, 1 mM EDTA) at 103,000 × *g* for 90 min at 4°C, using a TLA100.3 rotor in a Beckman Optima Max-E benchtop ultracentrifuge. Pellets were resuspended in PBS with 0.1 mg tRNA, and RNAs were extracted by phenol-chloroform treatment followed by ethanol precipitation. RNAs were then separated by 6% urea-PAGE and detected using a Silver Stain Plus kit (Bio-Rad) according to the manufacturer's instructions, except for the incorporation of a postfix oxidation step using 0.36% nitric acid (vol/vol) and 0.5% potassium dichromate (wt/vol). Experiments in which increasing quantities of vRNA were analyzed by this method and quantified by densitometry established that a linear relationship existed between vRNA staining intensity and the amount of nucleic acid over the concentration range used here (data not shown). As an alternative means for quantitative analysis of RNA content, aliquots (typically 150 to 300 μl) of clarified virus stock were mixed with 4,600 PFU of bacteriophage MS2, and RNAs were extracted using a QIAamp viral RNA kit (Qiagen). RNAs were eluted in 60 μl RNase-free water, and 5-μl aliquots were used to set up triplicate reactions for the detection of MS2 and either influenza A virus segment 5 or segment 7. Detection was done by quantitative RT-PCR (qRT-PCR), using the SuperScript III Platinum one-step qRT-PCR system (Invitrogen) and a Rotor-Gene 3000 real-time thermal cycler (Corbett Research Limited), and was carried out in accordance with UK National Standard method VSOP 25 (www.hpa-standardmethods.org.uk) for segment 7 and a derivative protocol for segment 5. Reaction conditions, primers, and TaqMan probe sequences are available upon request. Data were normalized by comparison with a dilution series of a PR8 virus of known titer; additional dilution series of the reverse genetic plasmids for segments 5 and 7, linearized with BglII, were used as standards to calculate the number of segments present in a sample.

RESULTS

Mutation of potential *cis*-acting RNA signals in segment 7 produces defective viruses. Previously, we sought to define *cis*-acting RNA signals in the coding regions of the influenza A virus genome at the nucleotide level by identifying regions of low codon diversity (17). Mutational studies guided by these bioinformatic data confirmed the ability of the analysis to identify conserved sequences involved in genome packaging (17, 27). These experiments primarily examined segment 1, so to further test the applicability of our approach, we used the bioinformatic data to guide the creation of synonymous mutations in conserved coding regions of segment 7. We hypothesized that such regions were likely to contribute to functionally important RNA elements. Attention was directed at the terminal regions of the segment (Fig. 1A) because although no prior experimental data on segment 7 packaging signals were available, extrapolation from the other seven segments (11, 12, 15, 16, 23, 35, 41, 50) suggested a likely role in genome packaging. Eight mutants were designed; half had changes to evolutionarily conserved codons, and half had changes in nearby, nonconserved codons as controls. The maximum number of synonymous changes (between two and five point mutations) was introduced into two or three adjacent conserved or nonconserved codons (Fig. 1B).

Although the bioinformatic analysis aimed to identify novel functional RNA sequences, it also identified known *cis*-acting sequences, such as splice donor and acceptor sequences (17).

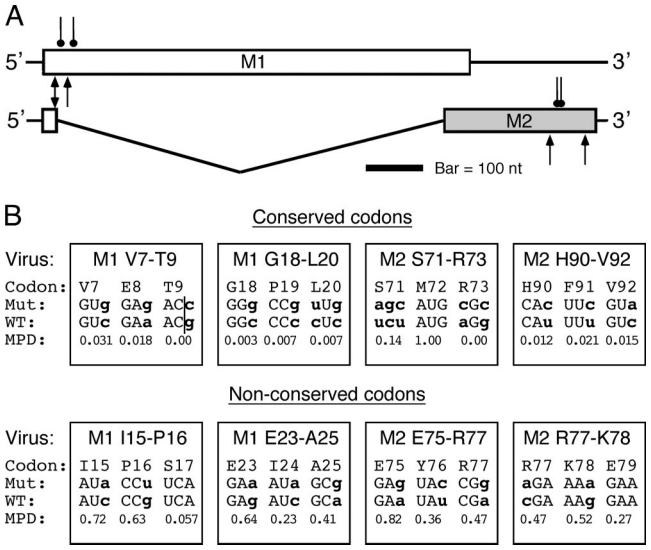

FIG. 1. Mutation of putative *cis*-acting signals in segment 7. (A) Scale diagram of segment 7 open reading frames and locations of introduced mutations in conserved codons (pointed arrows) and nonconserved codons (rounded arrows). (B) Nucleotide sequences (plus sense) of the codons altered in the indicated viruses. Mutations are shown in lowercase bold letters, and the mutant (Mut) and WT sequences are given. Also shown are the mean pairwise difference scores for each codon on a scale where 0 corresponds to absolute conservation of the codon and 1 corresponds to no conservation beyond that expected from amino acid constraint (17). The line in M1 V7-T9 indicates the position of the M2 splice site.

In general, the mutations were placed so as not to affect previously identified RNA functions. The exception to this was M1 V7-T9, where the mutations overlapped the 5′-splice donor of M2, altering the normally invariant G immediately 3′ of the splice site (Fig. 1B), a change expected to block splicing. Loss of M2 function is debilitating but not fatal to virus growth in tissue culture (5, 45, 49); thus, the M1 V7-T9 virus was expected to provide a baseline with which to gauge the severity of any defects resulting from the other mutations.

Mutations were introduced into a reverse genetic cDNA clone of PR8 segment 7 (8), and wild-type (WT) and mutant viruses were rescued by transfection of plasmids encoding this and the other seven segments into 293T cells. To assess the growth parameters of the viruses, stocks of the rescued viruses were grown in MDCK cells and titrated by plaque assay. Several independently rescued isolates of WT PR8 virus grew to titers of around 10^8 PFU/ml (Table 1). Mutant viruses with alterations to nonconserved codons replicated to very similar levels to those of the WT virus (plotted graphically in Fig. 2A; actual titer values are given in Table 1). However, viruses with alterations to conserved codons grew markedly less well, releasing between 10-fold (M2 H90-V92) and nearly 1,000-fold (M1 G18-L20) lower titers of PFU than the WT virus (Fig. 2A). Mutation of conserved codons also resulted in a statistically significant ($P < 0.001$) small-plaque phenotype in MDCK cells (Fig. 2B). To test for the presence of defective virions able to initiate a single but not multiple rounds of infection (as, for instance, might be expected if segment 7 were missing [28]), the infectious titers of the viruses were measured according to the ability of the viruses to express detectable levels of NP in individual cells at 8 h p.i. However, with one exception, the relative reductions in the ability of viruses with mutations in conserved regions to cause a single round of infection were similar to the relative reductions in their plaque titers (Fig. 2A). In the case of M1 V7-T9, the infectious titer was slightly greater than the plaque titer, but this was not statistically significant. The quantity of virus particles produced from infected cells was measured by HA assay. For viruses with mutations in conserved codons, this demonstrated relative growth defects similar to those observed by the plaque titers, again with the exception of M1 V7-T9, where the relative HA titer was slightly higher than the plaque titer (Fig. 2A). Together, these data show that synonymous changes to nonconserved codons in segment 7 have little effect on virus replication, but mutations in conserved regions are markedly deleterious to virus growth, lowering the output of infectious virus particles.

To examine the phenotypes of the mutants in a more physiological system, virus growth was assayed in embryonated chicken eggs. In this setting, the M1 E23-A25 mutant with changes to nonconserved codons grew similarly to the WT virus, whether replication was assessed by plaque, infectious, or HA titer (Fig. 2C and Table 2). The four viruses with alterations to conserved sequences showed similar drops in plaque titer relative to the WT virus to those for growth in MDCK cells, confirming their growth-defective phenotype. However, in contrast to their behavior in tissue culture, the relative infectious titers (as measured by the ability to express NP in a single cell) of the egg-grown defective viruses were substantially different from their relative plaque titers, displaying around 10-fold higher values (Fig. 2C). Additionally, the relative defects in particle release of these viruses (as mea-

TABLE 1. Plaque titers of MDCK-grown viruses

Virus	Titer (PFU/ml) in expt:				
	1	2	3	4	5
WT	3.8×10^7	7.3×10^8	6.2×10^8	2.6×10^8, 8.8×10^8	3.0×10^8
M1 V7-T9		1.1×10^6, 2.0×10^6		2.8×10^4	
M1 G18-L20		4.2×10^6		4.8×10^4	4.3×10^4
M2 S71-R73	1.2×10^6			3.1×10^7	8.0×10^6
M2 H90-V92			7.5×10^7		1.1×10^7
M1 I15-P16		5.5×10^8, 5.2×10^8			
M1 E23-A25			6.6×10^8		4.0×10^8
M2 E75-R77			6.0×10^8, 3.5×10^8		
M2 R77-K78		5.8×10^8, 6.2×10^8			

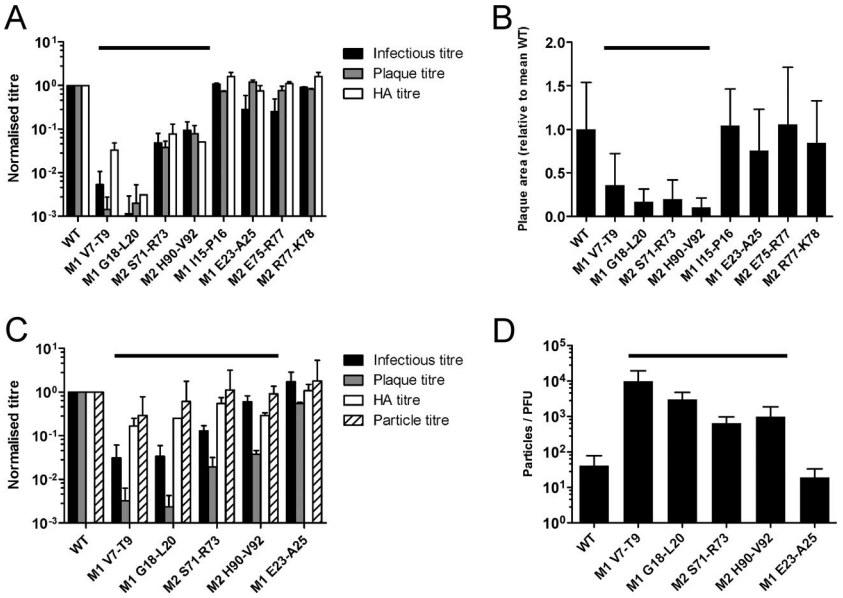

FIG. 2. Growth characteristics of viruses with mutations in the terminal coding regions of segment 7. Virus stocks were grown by low-multiplicity infection of MDCK cells (A and B) or eggs (C and D); viruses with changes to conserved codons are indicated by horizontal bars. (A and C) Virus growth was assessed by plaque assay, infectious center assay, HA assay, or EM particle counting (C and D). Values are plotted relative to the titer achieved by the WT virus in each experiment. The means plus standard deviations (SD) for three independently rescued virus stocks (for plaque and infectious titers of MDCK-grown M1 V7-T9, M1 G18-L20, and M2 S71-R73) or the means plus half-ranges for two virus stocks (for all other conditions) are shown. (B) Plaque size in MDCK cells was quantified and plotted relative to the mean area (+ SD) produced by infection with WT virus. Between 28 and 212 plaques were counted (mean, 93 plaques), depending on the virus. (D) The particle titers of egg-grown virus stocks were established by EM and used to derive particle/PFU ratios. The means plus half-ranges for two independent experiments are plotted.

sured by HA titer) were slight (<10-fold) compared to the particle release of the WT virus (Fig. 2C). To gain a more precise measure of virion production, the titer of released virus particles in the allantoic fluid was determined directly by particle counting (Fig. 2C). The particle counts were in good agreement with the HA assay data and confirmed that the defects in particle release were of a lesser magnitude than those observed in the matching plaque titers. In combination with the plaque assay data, we calculated particle/PFU ratios. The value for WT virus averaged around 40, in agreement with earlier studies (10, 43), while the control virus with mutations to nonconserved codons performed similarly (Fig. 2D). However, all four viruses with synonymous mutations in conserved terminal coding regions of the segment had particle/PFU ratios that were increased between 25- and 300-fold (Fig. 2D). Sequencing of segment 7 from each of the WT and mutant virus preparations from MDCK cells and eggs showed the presence of the designed mutations and no evidence of additional mutations (data not shown). Thus, synonymous mutations to conserved codons in the terminal regions of segment 7 caused defective viral growth in cell culture and in embryonated eggs, although the phenotypes of the viruses differed between the two systems. Growth in MDCK cells led to reduced amounts of released virus, while growth in eggs had less effect on the quantity of virus particles formed but dramatically reduced their specific infectivity.

TABLE 2. Plaque titers of egg-grown viruses

Virus	Titer (PFU/ml) in expt:	
	1	2
WT	1.8×10^9	1.3×10^9
M1 V7-T9	1.1×10^7	2.5×10^5
M1 G18-L20	7.5×10^6	5.0×10^5
M2 S71-R73	5.5×10^7	9.4×10^6
M2 H90-V92	8.0×10^7	3.7×10^7
M1 E23-A25	9.0×10^8	7.5×10^8

Effects of mutations on viral gene expression and RNA synthesis. With the exception of M1 V7-T9, which interferes with the 5′-splice donor site of M2, it was not anticipated that any

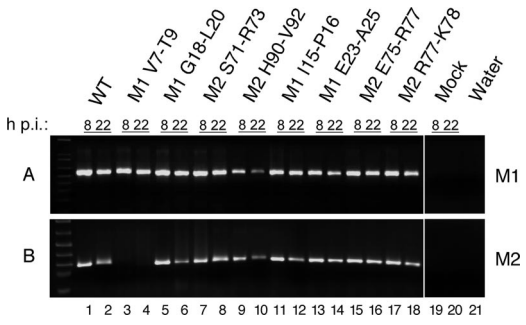

FIG. 3. Effects of synonymous mutations on viral mRNA synthesis. Total cell RNA was isolated from MDCK cells infected (or mock infected) with the indicated viruses at an MOI of 1 at 8 h or 22 h p.i., and M1 (A) or M2 (B) mRNA was detected by RT-PCR followed by agarose gel electrophoresis and staining with ethidium bromide. Water, PCRs carried out without a template.

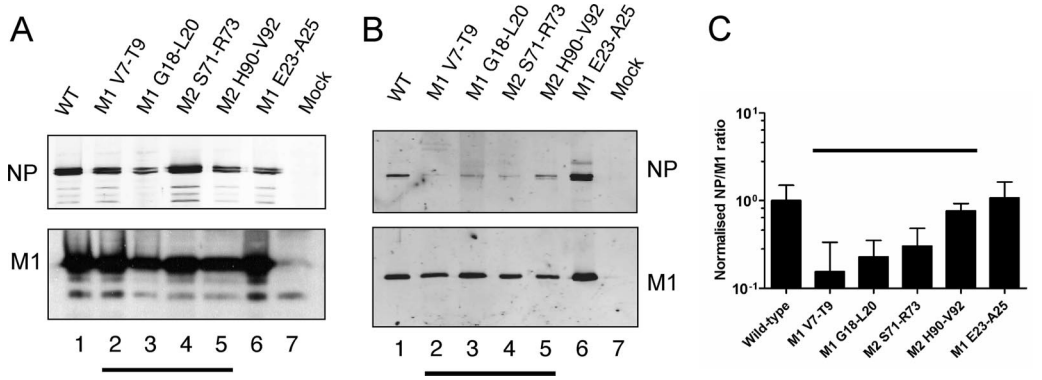

FIG. 4. Effects of synonymous mutations on M1 and NP expression and incorporation into virions. (A) Lysates from MDCK cells infected (or mock infected) at an MOI of 1 with the indicated viruses and harvested at 24 h p.i. were analyzed by SDS-PAGE and Western blotting for NP or M1, as labeled. (B) Approximately 1×10^9 virus particles from infected eggs were pelleted through a sucrose cushion, resuspended, and analyzed by SDS-PAGE and Western blotting for NP and M1. (C) The ratio of NP to M1 protein in two independently rescued egg-grown virus stocks was determined by densitometry of Western blots. Mean plus half-range values normalized with respect to those of WT virus are plotted; the bar indicates viruses with changes to conserved codons.

of the mutations would directly affect RNA or protein expression. Nevertheless, to control for possible pleiotropic effects, viral macromolecular synthesis was examined. To analyze segment 7 mRNA synthesis, RT-PCR analysis was carried out on total RNA isolated from cells infected with WT or defective virus and harvested at 8 h or 22 h p.i. Similar quantities of M1 mRNA were detected for most viruses (Fig. 3A). One possible exception was the M2 H90-V92 virus, which in some, but not all, experiments displayed a slight reduction in M1 mRNA (Fig. 3A, lanes 9 and 10). M2 mRNA was also produced normally in cells infected with all viruses, with the expected exception of M1 V7-T9, in which no expression was detectable (Fig. 3B). To assess viral protein synthesis, infected cell lysates were first examined by Western blotting. For all mutant viruses, M1 and NP proteins accumulated in infected cells at levels similar to those in WT virus (Fig. 4A). M2 expression was detected by immunofluorescence staining of infected cells, revealing similar intensities of staining for all viruses except M1 V7-T9, where no M2 was detectable, despite counterstaining for NP indicating successful infection (Fig. 5).

Next, we examined the effects of the mutations on vRNA synthesis. Relatively small amounts of vRNA (either segment 5 or 7) were detected in samples collected at 8 h p.i. from cells infected with the WT virus, while as expected, the quantities of both vRNAs had increased considerably at 22 h p.i. (Fig. 6A, lanes 1 and 2). No significant alteration to this pattern was seen with the defective viruses M1 V7-T9, M1 G18-L20, and M2 S71-R73 or the control virus M1 E23-A25 (Fig. 6A, lanes 3 to 8, 11, and 12). However, although exhibiting normal synthesis of segment 5, the M2 H90-V92 virus showed a consistent failure to amplify segment 7 vRNA at the late time point (Fig. 6A, lanes 9 and 10). In replicate experiments, accumulation of segment 7 (but not segment 5) vRNA was reduced about fivefold compared to that for the WT virus (Fig. 6B). Thus, the introduction of synonymous mutations into the conserved terminal coding regions of segment 7 had no effect on viral mac-

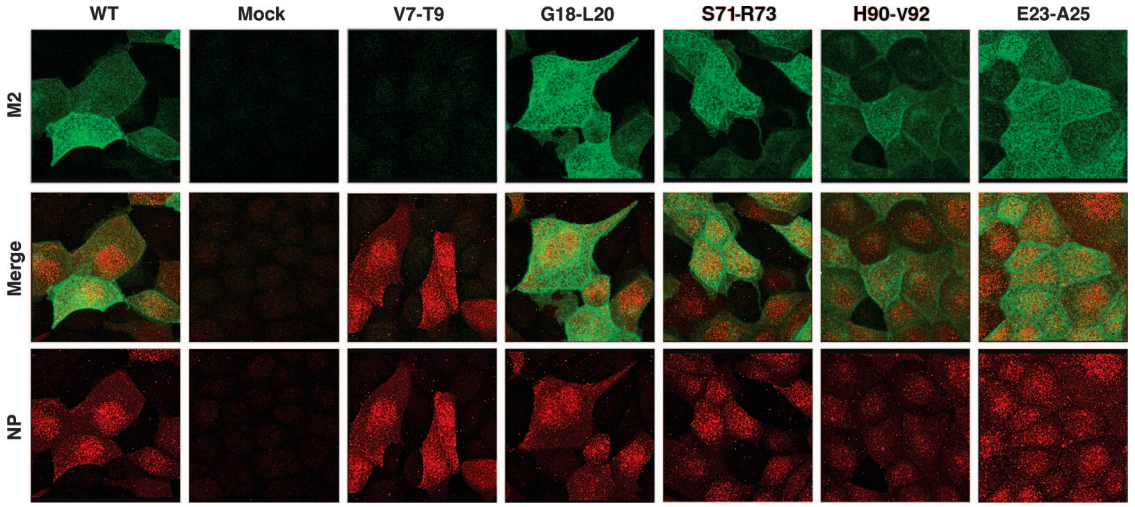

FIG. 5. M2 expression in WT and mutant virus-infected cells. MDCK cells were infected with the indicated viruses (or mock infected) at an approximate MOI of 1, fixed at 8 h p.i., and stained for M2 (green) and NP (red) by immunofluorescence.

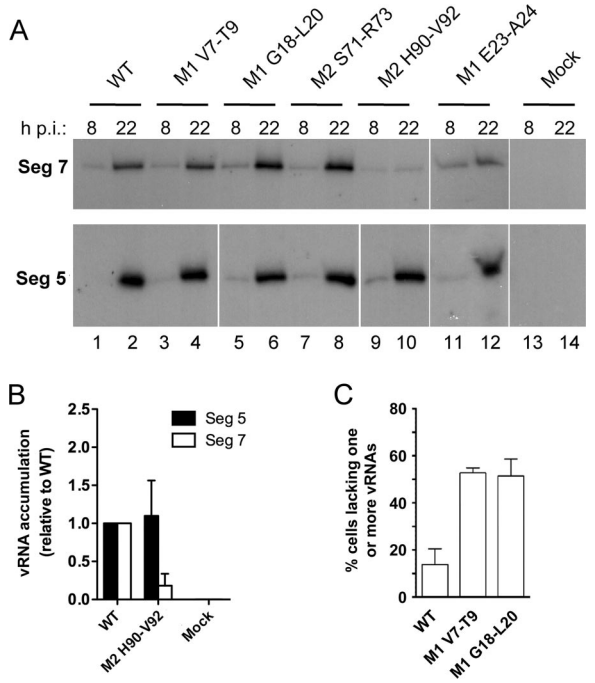

FIG. 6. Effects of synonymous mutations on vRNA synthesis. (A) vRNA contents of total RNAs isolated at 8 or 22 h p.i. from MDCK cells infected (or mock infected) with the indicated viruses at an MOI of 0.5 were determined by reverse transcriptase primer extension with oligonucleotides specific for segments 5 and 7. (B) Segment 5 and 7 vRNA accumulation at 22 h p.i. from WT and M2 H90-V92 viruses was quantified by densitometry. Means plus SD (for five independent experiments) are plotted relative to levels in WT virus-infected samples. (C) Expression of individual vRNAs in single infected cells. Cells were infected with the indicated viruses at an empirically determined dilution that resulted in not all cells expressing NP, fixed at 12 h p.i., and stained by immunofluorescence for NP and by FISH for either vRNA segments 7 and 2 or 5 and 8 (see the legend to Fig. 9 for further details). Cells were scored for the percentage of infected cells (defined as expressing NP protein) that failed to also express one or more of the vRNA segments stained by FISH. Data are plotted as means plus SD for four experiments, two stained for segments 2 and 7 and two stained for segments 5 and 8.

romolecular synthesis for the M1 G18-L20 or M2 S71-R73 mutant, while as expected, the M1 V7-T9 mutant failed to produce M2 mRNA and protein. Unexpectedly, M2 H90-V92 showed selectively reduced accumulation of segment 7 vRNA as well as possibly a minor decrease in the synthesis of segment 7 mRNA.

Synonymous mutations in segment 7 lead to defects in virion assembly. All four viruses with synonymous mutations in the conserved terminal coding regions of segment 7 showed significant growth defects in tissue culture and in eggs. In the case of M1 V7-T9 virus, this could plausibly be ascribed to its failure to express M2, while for M2 H90-V92, the reduction in segment 7 vRNA levels might play a role. However, the molecular basis for the poor replication of the M1 G18-L20 and M2 S71-R73 viruses was less obvious. To investigate the effects of the mutations on virion release, MDCK cells were infected at a high multiplicity, fixed at 8 h p.i., and imaged by transmission EM (Fig. 7A). For WT and M1 E23-A25 viruses, virions were seen budding in abundance from the plasma membranes of infected cells; with the defective mutants, budding viruses appeared to be less profuse. Although not quantitative, this confirms the inference from the HA titer data that viruses with mutations in conserved regions release fewer virions from infected MDCK cells and indicates that this was not due to a failure of assembled virions to detach from the plasma membrane. However, where virions were produced, they did not show obvious exterior morphological defects (Fig. 7A, insets) and in some cases showed the presence of dark staining in the virion interior indicative of RNPs (39). However, in our hands, the frequency of particles that clearly showed the distinctive 7+1 array of RNPs seen by other investigators (18, 39, 53) was not sufficiently high even in WT virus preparations to permit a numerical analysis of the content of mutant virions. EM of virion production from the chorioallantoic membranes of eggs was not attempted, but negative staining of virions found in the allantoic fluid showed them to also have apparently normal exterior morphology (Fig. 7B).

As the rationale of our study was to examine segment 7 packaging signals, we next examined the genome content of the egg-grown virus stocks. This was first assessed by measuring the amount of NP protein incorporated into virions. Egg-grown viruses were pelleted from allantoic fluid, and the protein contents of approximately equal numbers of particles (normalized by M1 content) were analyzed by Western blotting. The amounts of NP incorporated into three of the defective viruses were considerably smaller than that found in WT or control viruses (Fig. 4B). When the ratio of NP to M1 was measured from two independent sets of virus stocks, it was decreased around sixfold in the case of M1 V7-T9 virus and around three- to fourfold for the M1 G18-L20 and M2 S71-R73 viruses (Fig. 4C). NP is the major protein component of RNP complexes (42), so for these viruses, a lack of NP implies a reduction in total genome content.

To detect genomic RNA directly, virus was pelleted from allantoic fluid, and vRNAs were extracted and quantified by qRT-PCR for segments 5 and 7. In combination with DNA standards of known concentrations and the previously determined particle titers of the viruses, this allowed the determination of the average number of segments per virion. The values so calculated for WT virus were around 5 copies per particle (data not shown), in reasonable agreement with the expected value of 1; the discrepancy probably reflects systematic errors in the particle counting process and/or qRT-PCR quantification. Accordingly, the values obtained for the mutant viruses were normalized with respect to WT virus levels. For the control virus M1 E23-A25, with mutations to nonconserved codons, the values obtained were close to those for the WT virus (Fig. 8A). In contrast, the three most defective viruses with alterations to conserved codons had substantially fewer copies of each segment per particle than WT virus did, with the number of copies of each segment incorporated by M1 V7-T9 being less than 1/10 of WT levels and M1 G18-L20 and M2 S71-R73 containing around 1/3 of the WT number of segments (Fig. 8A). The M2 H90-V92 virus also showed a reduction in vRNA content compared to the WT virus, but this was less than those for the other mutants. In all cases, however, it was noticeable that although the mutations were introduced into segment 7, incorporation of segment 5 was also reduced proportionally. To determine if this was matched by similar re-

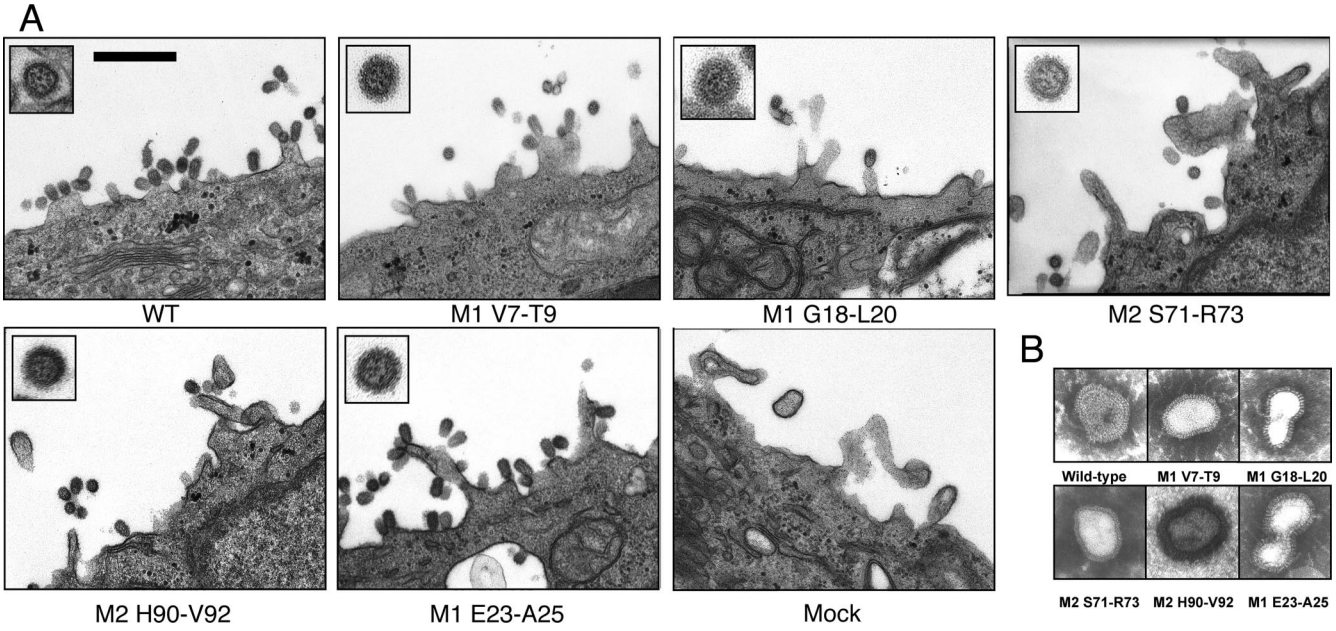

FIG. 7. EM analysis of virus budding and assembly. (A) MDCK cells were infected (or mock infected) with the indicated viruses at an MOI of 4 and fixed at 8 h p.i. before analysis by transmission EM. Bar, 500 nm. Insets show individual virions at an increased magnification. (B) Egg-grown virus was purified and examined by negative stain transmission EM. Representative virions are shown.

ductions in the contents of the other six segments, we examined the RNA content of virions directly by urea-PAGE and silver staining. When RNAs were extracted from equal numbers of virus particles, the overall amounts obtained from the viruses with mutations to conserved codons (as determined by densitometry) were reduced over sevenfold for virus M1 V7-T9 and three- to fourfold for the other three viruses, confirming the lower yields seen by qRT-PCR. However, when the RNA samples were normalized before PAGE analysis to take this into account, RNA species with the expected relative mobilities for the full complement of eight vRNA molecules were visible at similar staining intensities in all cases, i.e., from WT virus, the phenotypically normal M1 E23-A25 mutant, and the four defective viruses (Fig. 8B, lanes 1 to 6). A sample derived from an equivalent quantity of uninfected allantoic fluid was devoid of any apparent staining (lane 7). Thus, no individual segment appeared to be lost specifically from any of the mutant viruses. Densitometry of replicate gels indicated no more than a twofold deviation from apparent equimolar packaging (data not shown), suggesting that the matching reductions in packaging of segments 5 and 7 seen by qRT-PCR were indeed accompanied by similar reductions of all genome segments.

As an alternative method of assessing the specific infectivity of the viruses, independent of EM particle counting, the qRT-PCR data were plotted with reference to the plaque titers of the virus stocks, thus displaying the relative numbers of input

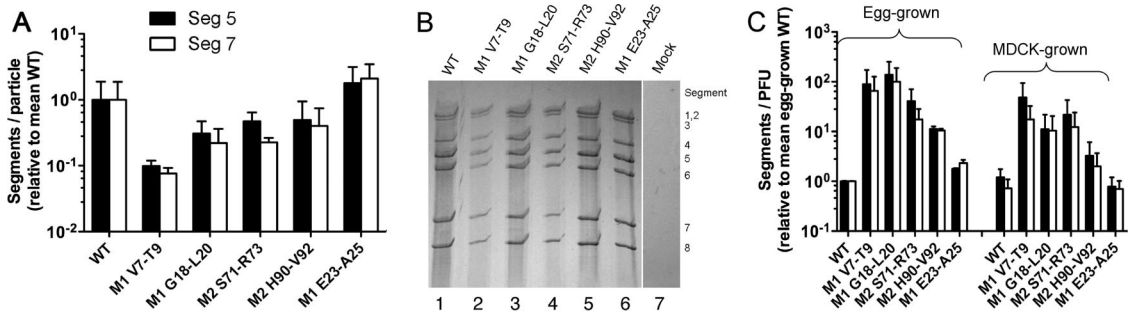

FIG. 8. Effects of synonymous mutations on segment packaging. (A and C) RNAs were extracted from the allantoic fluid of infected eggs or the culture medium of infected MDCK cells, and segment 5 and 7 vRNA contents were determined by qRT-PCR. Segment concentrations were calculated with respect to plasmid standards. (A) The matching particle titers (Fig. 2) were used to calculate segment/particle ratios that were then normalized with respect to that seen for the WT virus. The mean plus half-range values for two independently rescued virus stocks are shown. (B) Egg-grown virions were pelleted from infected allantoic fluid, and approximately equal amounts of RNA (corresponding to approximately 6×10^9 WT virus particles) were separated by urea-PAGE and detected by silver staining (lanes 1 to 6). Mock-infected allantoic fluid was analyzed in parallel (lane 7). (C) Plaque titer data (Fig. 2) were used to calculate the segment/PFU ratios of the indicated viruses. Values were normalized to those of the WT egg-grown virus. The means and half-ranges for two independently rescued virus stocks are shown (except for MDCK-grown WT virus, for which the mean and SD for three independent isolates are plotted).

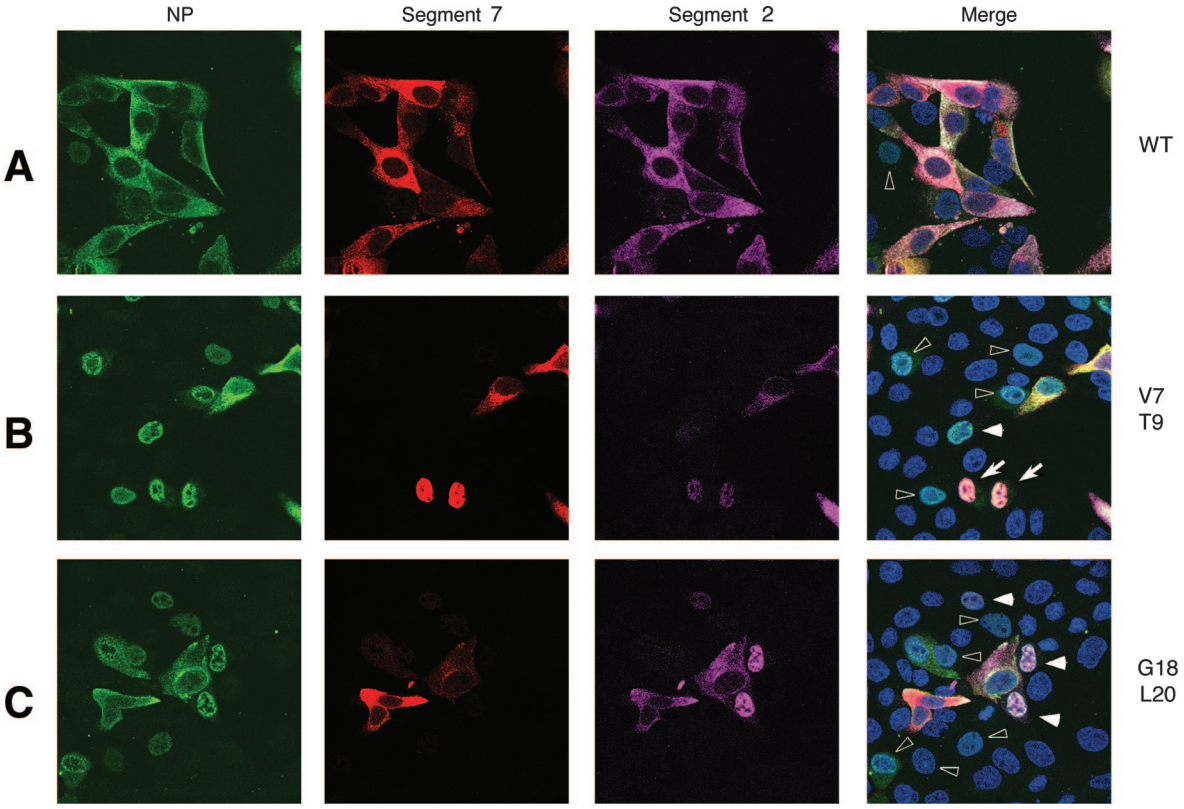

FIG. 9. FISH analysis of vRNA content of individual infected cells. MDCK cells were infected with the indicated viruses at an empirically determined dilution that resulted in not all cells expressing NP. Cells were fixed at 12 h p.i. and stained by immunofluorescence for NP (green) and by FISH for segments 7 (red) and 2 (magenta). Nuclei were stained with DAPI (4′,6-diamidino-2-phenylindole) (blue). Open arrowheads highlight cells expressing only NP protein, filled arrowheads show those expressing NP and a single vRNA, and arrows show cells expressing NP and both vRNAs, but with nuclear export failing to occur.

segments needed to successfully initiate a plaque. Values for the WT and control M1 E23-A25 viruses (grown in eggs) were similar (Fig. 8C, left panel). The defective virus stocks, however, packaged between 10- and 100-fold larger numbers of segments for each PFU (Fig. 8C), confirming their dramatically increased particle/PFU ratios (Fig. 2D). We were unable to get reliable particle counts for the mutant virus stocks grown in MDCK cells because in this system the defective viruses released far fewer particles than the WT virus did (Fig. 2A). However, the better sensitivity of the qRT-PCR method allowed the measurement of segment/PFU ratios for these viruses. Like the case for those grown in eggs, the three most defective viruses showed notable increases in the numbers of segments required to initiate a multicycle infection compared to fully replication-competent viruses, although these increases were not as high as those for the egg-grown viruses (Fig. 8C, right panel). Thus, although the primary effect of the segment 7 mutations on virus growth in MDCK cells was to inhibit particle assembly, those virions that were formed also had a lower specific infectivity than that of WT virions, similar to the mutant phenotype in eggs.

Thus, synonymous mutations within conserved segment 7 coding regions led to packaging defects in which the populations of mutant particles contained lower than expected but approximately equimolar quantities of each segment. However, in relative terms, the underincorporation of the genome was slight compared to the magnitudes of the deficits in overall virus replication and particle/PFU or segment/PFU ratios, i.e., there were approximately 3- to 10-fold reductions in genome content (Fig. 8A) versus 10- to 400-fold changes in plaque titers (Fig. 2C) and particle/PFU ratios (Fig. 2D) or segment/PFU ratios (Fig. 8C). To explain this, we hypothesized that the mutations disrupted the packaging mechanism to such an extent that a minority of virions contained one copy of all eight segments and the majority contained an imperfect selection with a mean number of substantially less than 8. To test this hypothesis, we infected cells at a low MOI and at 12 h p.i. examined their ability to successfully express NP protein by immunofluorescence and to amplify pairs of vRNA segments by FISH. The latter step requires the presence of genes for the three polymerase proteins and NP (the minimal requirements for genome replication) (19, 47) as well as whatever additional segments are under analysis. Expression of NP protein requires only the presence of segment 5, as primary mRNA transcription produces substantial amounts of gene expression even in the absence of vRNA amplification (2, 7, 25). In cells infected with WT virus, most cells that expressed detectable levels of NP protein also contained substantial quantities of segments 2 and 7 that, as expected for a late time point, were predominantly cytoplasmic (Fig. 9A). Even with WT virus, however, some cells were apparently abortively infected and contained only NP protein that was retained in the nucleus

(Fig. 9A). However, in cells infected with either of the two most defective viruses, infected cells that stained positively for all three viral macromolecules were in the minority. The majority contained nuclear NP staining with either no detectable vRNA (Fig. 9B and C), only a single segment, or both vRNAs retained in the nucleus, indicating an abortive infection for other reasons. Essentially identical results were obtained when cells were stained for NP and vRNAs for segments 5 and 8 (data not shown). When individual NP-expressing cells from replicate experiments were scored according to whether infection had proceeded normally, with evident expression of both vRNAs under examination, it was apparent that the mutant viruses initiated a far larger proportion of abortive infections that failed to detectably express one or more vRNA molecules (Fig. 6C). This behavior is consistent with the hypothesis that the synonymous mutations in segment 7 disrupt packaging to the extent that significant numbers of infectious but defective particles containing an incomplete genome are formed.

DISCUSSION

Having previously identified regions of codon conservation in the influenza A virus genome (17), we show here that introducing even a small number of synonymous changes into such regions of segment 7, in an otherwise WT background, renders the virus profoundly defective. The mutations chosen did not substantially increase the use of codons that are rare in influenza A virus genomes (17) or canine and chicken genomes (http://www.kazusa.or.jp/codon/) or the number of unfavorable codon pairs (6). We aimed to define segment-specific packaging signals, and the consistent outcome of a phenotype of poorly infective particles with defects in vRNA content suggests that we were successful. Segment 7 was (to the best of our knowledge) the last influenza A virus genomic segment for which no published experimental information was available regarding the presence or location of packaging signals, either from direct mapping experiments or inferred from the structure of defective interfering RNAs. Although our mutational strategy was not exhaustive, the fact that mutations located in the terminal coding regions disrupted packaging, coupled with our previous bioinformatic approach (17), strongly suggests that like all other segments, segment 7 contains packaging signals located toward the 5′ and 3′ ends of the vRNA coding regions.

With the exception of a mutation expected to disrupt the 5′ splice donor site for the M2 mRNA (M1 V7-T9), none of the alterations targeted RNA sequences with known function. However, two of the mutants had phenotypes suggestive of pleiotropy. The M1 V7-T9 virus replicated poorly (Fig. 2) and had the most severe packaging defect in terms of its segment/particle ratio (Fig. 8A), and while this is consistent with other work showing the importance of M2 for particle assembly and genome packaging (20, 31, 32), we suspect that the lack of M2 was not the only defect at play. Supporting this, an MDCK cell line that constitutively expresses M2 (46) did not complement the growth of M1 V7-T9 virus, whereas growth of a virus whose M2 expression was abolished by stop codons in exon 2, well away from the segment termini, was increased 10,000-fold (data not shown) (ΔM2 virus and MDCK-M2 cells were a kind gift from W. Barclay). Thus, it appears that this small region of RNA fulfils at least four separate but overlapping roles, as part of an open reading frame for two proteins, as a splice donor site, and as a packaging signal. In further evidence of pleiotropy, the M2 H90-V92 virus was unexpectedly and specifically deficient in the accumulation of segment 7 vRNA. The reason for this deficiency is unknown. It could in principle be due to a defect in segment 7 vRNA or cRNA synthesis or to a reduction in the stability of either RNA species. Although mutations in the unique regions of segments have previously been shown to affect vRNA synthesis (3, 55), these alterations were in the untranslated regions and closer to the core promoter sequences than those in virus M2 H90-V92, which are a further 15 to 21 nucleotides in from the untranslated region. This is similar to the behavior of two synonymous point mutations in a segment 1-derived reporter construct that reduced vRNA accumulation in a mini-replicon system between three- and fivefold, despite lying nearly 60 nucleotides into the coding region (17). In all of these cases, the lowered accumulation of the mutant segments did not affect the efficiency with which they were packaged into virus (3, 17), and in counterpoint, it seems unlikely that the reduced accumulation of segment 7 in the M2 H90-V92 virus is the only reason for its poor replication. Although it was the least severely affected virus, like the other three viruses with alterations to conserved codons, it also showed increased particle/PFU and segment/PFU ratios and a decrease in overall packaged vRNA content, suggesting that it too has a packaging defect. Thus, it is plausible that there are multiple overlapping RNA functions in this mutated region as well. Overall, these data highlight the functional complexity of the influenza virus genome.

Experiments utilizing deletion mapping studies of the uptake of engineered reporter vRNA molecules provide compelling evidence that segment-specific packaging signals exist but have not elucidated the means by which they function (9, 11, 15, 16, 23, 35, 41, 50). Like others, we reasoned that studying the behavior of otherwise normal viruses with synonymous lesions in individual segments that specifically affected segment packaging would be informative. So far, studies have applied this strategy to segments 1 to 4 and 8 (15, 24, 26, 27). It is therefore interesting to compare our results for segment 7 with these prior data. One strikingly consistent finding is that relatively small changes to packaging signals (in many cases with no evidence of nonspecific effects on other aspects of virus replication) can profoundly inhibit virus replication. Reductions in titer to 0.1 to 1% of WT levels resulted from synonymous alterations of between 3 and 14 nucleotides in segment 7 (virus M1 G18-L20 [this study]) and in segments 1 to 3 (24, 27). Indeed, in our hands, mutation of as few as four nucleotides within segment 7 caused as profound a defect in virus replication as the loss of M2 expression. Other changes within these segments or within segment 4 or 8 had lesser effects but still reduced virus replication up to 10-fold (15, 26). The effect of mutating a particular segment on packaging of it and the other segments was less consistent, however. Most mutations to segments 1 to 3 that reduced overall virus replication also resulted in nonequimolar packaging of the vRNAs, with disproportionate reductions (for segments 1 and 2) in the packaging of the mutated segment (27). In the case of segment 1, many (but not all) mutations also substantially reduced packaging of all segments except for segments 4 and 6 (27). When segment 3 was

mutated, incorporation of segments 1 and 5 was apparently more affected than that of segment 3 itself (27). In contrast, mutation of packaging signals in segments 4 and 7 had little effect on the stoichiometry of segment incorporation into the virus population, with generally <2-fold changes in the proportion of any individual segment (26 [segment 4]; this study [segment 7]). Marsh and colleagues did not examine the numbers of particles formed by their mutant viruses, but we show here that the apparently equimolar vRNA incorporation in the presence of a mutated segment 7 in fact resulted from a reduction in packaging of all eight segments (Fig. 8A). The observation that WT virus particles do not commonly incorporate more than eight vRNAs (22, 37, 39), in conjunction with the relative reductions in genome content of the mutant viruses, strongly suggests that, on average, the viruses contained substantially fewer than eight segments per particle, consistent with the evident lack of one or more vRNAs in the majority of cells infected by the M1 V7-T9 and M1 G18-L20 viruses (Fig. 6C and 9). Interpreting this result in light of the prevailing hypothesis that packaging signals operate by mediating a web of specific intersegment RNA-RNA interactions that assemble a tightly apposed array of all eight vRNAs (16, 17, 39) suggests that segment 7 plays a major role in this process because mutations to a single segment have disrupted packaging of most, if not all, segments. In the case of the M1 V7-T9 and M1 G18-L20 viruses, the severity of the packaging defect is such that the increases in particle/PFU ratio relative to that of the WT virus approach that predicted for a purely random packaging process (22, 37) (around 2 $\log_{10}$ worse than that of the WT virus). Other possibilities, such as pseudo-random packaging resulting from incorporation of specific subcomplexes of segments that, in aggregate, appear equimolar, are also compatible with the data. Based on the efficiency with which hybrid reporter vRNA constructs supported the formation of virus-like particles, Muramoto and colleagues concluded that segment 1 exerted a particularly important influence on packaging of other segments (35). We note, however, that if one considers the small numbers of virus-like particles formed in their experiments in the absence of segment 7 or any likely segment 7 packaging signals, the data suggest an equal importance for segment 7, consistent with our findings. It may be that further analyses of this type, applied to other segments, will permit a fuller model of these putative segment interactions to be built up. Ultimate confirmation (or refutation) of the RNA-RNA interaction model for packaging will, however, require other experimental approaches.

Several studies have noted that the loss of an individual segment or the deletion of functionally important regions of its packaging signals reduces the number of particles released from cultured cells (9, 16, 23, 35). We confirmed and extended this observation by showing that mutation of as few as four nucleotides is sufficient to inhibit particle formation from MDCK cells by over 99% (Fig. 2A). For the mutants described here, it is notable that viral proteins were synthesized normally in infected MDCK cells, yet there was no evidence for an accumulation of virions that were stalled at the plasma membrane due to a defect in the pinching-off process (as seen, for example, during lipid raft perturbation [48]). One possibility, therefore, is that assembly of a higher-order RNP complex somehow promotes the budding process in mammalian cells. Interestingly, however, the inhibitory effect of the packaging mutations on virus budding was far less marked when the viruses were grown in embryonated eggs, with particle or HA titers decreasing <10-fold (Fig. 2C). Although the production of viable virus particles by the mutants was equally low in the two systems, the tendency in eggs was to produce greater numbers of defective particles than those produced from cultured cells (Fig. 2A and C and 9C). Comparison of published results (9, 16, 23, 35) indicates that reduced levels of virus budding in the absence of normal packaging signals are consistent for at least MDCK and 293T cells, but we have not yet tested whether the altered behavior of our mutants in eggs is specific to the tissue used or reflects a general feature of avian cells. We previously suggested that incompatibilities between packaging signals from different strains of virus will influence the process of genome reassortment (17). The finding here that small sequence alterations can profoundly affect virus fitness is consistent with this hypothesis. The possibility that cell type or species also affects the process of virus reassortment has significant implications for influenza A virus evolution and is worth investigating further.

ACKNOWLEDGMENTS

We thank Emmie de Wit and Ron Fouchier for the PR8 reverse genetic system, Wendy Barclay for discussions and reagents, and Laurence Tiley and Helen Wise for critiquing the work.

This work was supported by a grant from the Medical Research Council (G0700815) to P.D. E.C.H. and E.K.R. are supported by studentships from the Wellcome Trust.

REFERENCES

1. **Abramoff, M. D., P. J. Magelhaes, and S. J. Ram.** 2004. Image processing with ImageJ. Biophotonics Int. **11:**36–42.
2. **Amorim, M. J., E. K. Read, R. M. Dalton, L. Medcalf, and P. Digard.** 2007. Nuclear export of influenza A virus mRNAs requires ongoing RNA polymerase II activity. Traffic **8:**1–11.
3. **Bergmann, M., and T. Muster.** 1996. Mutations in the nonconserved noncoding sequences of the influenza A virus segments affect viral vRNA formation. Virus Res. **44:**23–31.
4. **Chao, L., T. T. Tran, and T. T. Tran.** 1997. The advantage of sex in the RNA virus phi6. Genetics **147:**953–959.
5. **Cheung, T. K., Y. Guan, S. S. Ng, H. Chen, C. H. Wong, J. S. Peiris, and L. L. Poon.** 2005. Generation of recombinant influenza A virus without M2 ion-channel protein by introduction of a point mutation at the 5′ end of the viral intron. J. Gen. Virol. **86:**1447–1454.
6. **Coleman, J. R., D. Papamichail, S. Skiena, B. Futcher, E. Wimmer, and S. Mueller.** 2008. Virus attenuation by genome-scale changes in codon pair bias. Science **320:**1784–1787.
7. **Dalton, R. M., A. E. Mullin, M. J. Amorim, E. Medcalf, L. S. Tiley, and P. Digard.** 2006. Temperature sensitive influenza A virus genome replication results from low thermal stability of polymerase-cRNA complexes. Virol. J. **3:**58.
8. **de Wit, E., M. I. Spronken, T. M. Bestebroer, G. F. Rimmelzwaan, A. D. Osterhaus, and R. A. Fouchier.** 2004. Efficient generation and growth of influenza virus A/PR/8/34 from eight cDNA fragments. Virus Res. **103:**155–161.
9. **de Wit, E., M. I. Spronken, G. F. Rimmelzwaan, A. D. Osterhaus, and R. A. Fouchier.** 2006. Evidence for specific packaging of the influenza A virus genome from conditionally defective virus particles lacking a polymerase gene. Vaccine **24:**6647–6650.
10. **Donald, H. B., and A. Isaacs.** 1954. Counts of influenza virus particles. J. Gen. Microbiol. **10:**457–464.
11. **Dos Santos Afonso, E., N. Escriou, I. Leclercq, S. van der Werf, and N. Naffakh.** 2005. The generation of recombinant influenza A viruses expressing a PB2 fusion protein requires the conservation of a packaging signal overlapping the coding and noncoding regions at the 5′ end of the PB2 segment. Virology **341:**34–46.
12. **Duhaut, S., and N. J. Dimmock.** 2000. Approximately 150 nucleotides from the 5′ end of an influenza A segment 1 defective virion RNA are needed for genome stability during passage of defective virus in infected cells. Virology **275:**278–285.
13. **Duhaut, S. D., and J. W. McCauley.** 1996. Defective RNAs inhibit the

assembly of influenza virus genome segments in a segment-specific manner. Virology **216:**326–337.
14. **Elton, D., M. Simpson-Holley, K. Archer, L. Medcalf, R. Hallam, J. McCauley, and P. Digard.** 2001. Interaction of the influenza virus nucleoprotein with the cellular CRM1-mediated nuclear export pathway. J. Virol. **75:**408–419.
15. **Fujii, K., Y. Fujii, T. Noda, Y. Muramoto, T. Watanabe, A. Takada, H. Goto, T. Horimoto, and Y. Kawaoka.** 2005. Importance of both the coding and the segment-specific noncoding regions of the influenza A virus NS segment for its efficient incorporation into virions. J. Virol. **79:**3766–3774.
16. **Fujii, Y., H. Goto, T. Watanabe, T. Yoshida, and Y. Kawaoka.** 2003. Selective incorporation of influenza virus RNA segments into virions. Proc. Natl. Acad. Sci. USA **100:**2002–2007.
17. **Gog, J. R., S. Afonso Edos, R. M. Dalton, I. Leclercq, L. Tiley, D. Elton, J. C. von Kirchbach, N. Naffakh, N. Escriou, and P. Digard.** 2007. Codon conservation in the influenza A virus genome defines RNA packaging signals. Nucleic Acids Res. **35:**1897–1907.
18. **Harris, A., G. Cardone, D. C. Winkler, J. B. Heymann, M. Brecher, J. M. White, and A. C. Steven.** 2006. Influenza virus pleiomorphy characterized by cryoelectron tomography. Proc. Natl. Acad. Sci. USA **103:**19123–19127.
19. **Huang, T. S., P. Palese, and M. Krystal.** 1990. Determination of influenza virus proteins required for genome replication. J. Virol. **64:**5669–5673.
20. **Iwatsuki-Horimoto, K., T. Horimoto, T. Noda, M. Kiso, J. Maeda, S. Watanabe, Y. Muramoto, K. Fujii, and Y. Kawaoka.** 2006. The cytoplasmic tail of the influenza A virus M2 protein plays a role in viral assembly. J. Virol. **80:**5233–5240.
21. **Jennings, P. A., J. T. Finch, G. Winter, and J. S. Robertson.** 1983. Does the higher order structure of the influenza virus ribonucleoprotein guide sequence rearrangements in influenza viral RNA? Cell **34:**619–627.
22. **Laver, W. G., and J. C. Downie.** 1976. Influenza virus recombination. I. Matrix protein markers and segregation during mixed infections. Virology **70:**105–117.
23. **Liang, Y., Y. Hong, and T. G. Parslow.** 2005. *cis*-Acting packaging signals in the influenza virus PB1, PB2, and PA genomic RNA segments. J. Virol. **79:**10348–10355.
24. **Liang, Y., T. Huang, H. Ly, T. G. Parslow, and Y. Liang.** 2008. Mutational analyses of packaging signals in influenza virus PA, PB1, and PB2 genomic RNA segments. J. Virol. **82:**229–236.
25. **Mark, G. E., J. M. Taylor, B. Broni, and R. M. Krug.** 1979. Nuclear accumulation of influenza viral RNA transcripts and the effects of cycloheximide, actinomycin D, and alpha-amanitin. J. Virol. **29:**744–752.
26. **Marsh, G. A., R. Hatami, and P. Palese.** 2007. Specific residues of the influenza A virus hemagglutinin viral RNA are important for efficient packaging into budding virions. J. Virol. **81:**9727–9736.
27. **Marsh, G. A., R. Rabadan, A. J. Levine, and P. Palese.** 2008. Highly conserved regions of influenza A virus polymerase gene segments are critical for efficient viral RNA packaging. J. Virol. **82:**2295–2304.
28. **Martin, K., and A. Helenius.** 1991. Nuclear transport of influenza virus ribonucleoproteins: the viral matrix protein (M1) promotes export and inhibits import. Cell **67:**117–130.
29. **Martin-Benito, J., E. Area, J. Ortega, O. Llorca, J. M. Valpuesta, J. L. Carrascosa, and J. Ortin.** 2001. Three-dimensional reconstruction of a recombinant influenza virus ribonucleoprotein particle. EMBO Rep. **2:**313–317.
30. **Matrosovich, M., T. Matrosovich, W. Garten, and H. D. Klenk.** 2006. New low-viscosity overlay medium for viral plaque assays. Virol. J. **3:**63.
31. **McCown, M. F., and A. Pekosz.** 2006. Distinct domains of the influenza A virus M2 protein cytoplasmic tail mediate binding to the M1 protein and facilitate infectious virus production. J. Virol. **80:**8178–8189.
32. **McCown, M. F., and A. Pekosz.** 2005. The influenza A virus M2 cytoplasmic tail is required for infectious virus production and efficient genome packaging. J. Virol. **79:**3595–3605.
33. **Moya, A., E. C. Holmes, and F. Gonzalez-Candelas.** 2004. The population genetics and evolutionary epidemiology of RNA viruses. Nat. Rev. Microbiol. **2:**279–288.
34. **Mullin, A. E., R. M. Dalton, M. J. Amorim, D. Elton, and P. Digard.** 2004. Increased amounts of the influenza virus nucleoprotein do not promote higher levels of viral genome replication. J. Gen. Virol. **85:**3689–3698.
35. **Muramoto, Y., A. Takada, K. Fujii, T. Noda, K. Iwatsuki-Horimoto, S. Watanabe, T. Horimoto, H. Kida, and Y. Kawaoka.** 2006. Hierarchy among viral RNA (vRNA) segments in their role in vRNA incorporation into influenza A virions. J. Virol. **80:**2318–2325.
36. **Murti, K. G., W. J. Bean, Jr., and R. G. Webster.** 1980. Helical ribonucleoproteins of influenza virus: an electron microscopic analysis. Virology **104:**224–229.
37. **Nakajima, K., and A. Sugiura.** 1977. Three-factor cross of influenza virus. Virology **81:**486–489.
38. **Ng, A. K., H. Zhang, K. Tan, Z. Li, J. H. Liu, P. K. Chan, S. M. Li, W. Y. Chan, S. W. Au, A. Joachimiak, T. Walz, J. H. Wang, and P. C. Shaw.** 2008. Structure of the influenza virus A H5N1 nucleoprotein: implications for RNA binding, oligomerization, and vaccine design. FASEB J. **22:**3638–3647.
39. **Noda, T., H. Sagara, A. Yen, A. Takada, H. Kida, R. H. Cheng, and Y. Kawaoka.** 2006. Architecture of ribonucleoprotein complexes in influenza A virus particles. Nature **439:**490–492.
40. **Noton, S. L., E. Medcalf, D. Fisher, A. E. Mullin, D. Elton, and P. Digard.** 2007. Identification of the domains of the influenza A virus M1 matrix protein required for NP binding, oligomerization and incorporation into virions. J. Gen. Virol. **88:**2280–2290.
41. **Ozawa, M., K. Fujii, Y. Muramoto, S. Yamada, S. Yamayoshi, A. Takada, H. Goto, T. Horimoto, and Y. Kawaoka.** 2007. Contributions of two nuclear localization signals of influenza A virus nucleoprotein to viral replication. J. Virol. **81:**30–41.
42. **Portela, A., and P. Digard.** 2002. The influenza virus nucleoprotein: a multifunctional RNA-binding protein pivotal to virus replication. J. Gen. Virol. **83:**723–734.
43. **Schulze, I. T.** 1972. The structure of influenza virus. II. A model based on the morphology and composition of subviral particles. Virology **47:**181–196.
44. **Simpson-Holley, M., D. Ellis, D. Fisher, D. Elton, J. McCauley, and P. Digard.** 2002. A functional link between the actin cytoskeleton and lipid rafts during budding of filamentous influenza virions. Virology **301:**212–225.
45. **Takeda, M., A. Pekosz, K. Shuck, L. H. Pinto, and R. A. Lamb.** 2002. Influenza A virus M2 ion channel activity is essential for efficient replication in tissue culture. J. Virol. **76:**1391–1399.
46. **Thomas, J. M., M. P. Stevens, N. Percy, and W. S. Barclay.** 1998. Phosphorylation of the M2 protein of influenza A virus is not essential for virus viability. Virology **252:**54–64.
47. **Vreede, F. T., T. E. Jung, and G. G. Brownlee.** 2004. Model suggesting that replication of influenza virus is regulated by stabilization of replicative intermediates. J. Virol. **78:**9568–9572.
48. **Wang, X., E. R. Hinson, and P. Cresswell.** 2007. The interferon-inducible protein viperin inhibits influenza virus release by perturbing lipid rafts. Cell Host Microbe **2:**96–105.
49. **Watanabe, T., S. Watanabe, H. Ito, H. Kida, and Y. Kawaoka.** 2001. Influenza A virus can undergo multiple cycles of replication without M2 ion channel activity. J. Virol. **75:**5656–5662.
50. **Watanabe, T., S. Watanabe, T. Noda, Y. Fujii, and Y. Kawaoka.** 2003. Exploitation of nucleic acid packaging signals to generate a novel influenza virus-based vector stably expressing two foreign genes. J. Virol. **77:**10575–10583.
51. **Webby, R. J., and R. G. Webster.** 2003. Are we ready for pandemic influenza? Science **302:**1519–1522.
52. **Webster, R. G., W. J. Bean, O. T. Gorman, T. M. Chambers, and Y. Kawaoka.** 1992. Evolution and ecology of influenza A viruses. Microbiol. Rev. **56:**152–179.
53. **Yamaguchi, M., R. Danev, K. Nishiyama, K. Sugawara, and K. Nagayama.** 2008. Zernike phase contrast electron microscopy of ice-embedded influenza A virus. J. Struct. Biol. **162:**271–276.
54. **Ye, Q., R. M. Krug, and Y. J. Tao.** 2006. The mechanism by which influenza A virus nucleoprotein forms oligomers and binds RNA. Nature **444:**1078–1082.
55. **Zheng, H., P. Palese, and A. Garcia-Sastre.** 1996. Nonconserved nucleotides at the 3′ and 5′ ends of an influenza A virus RNA play an important role in viral RNA replication. Virology **217:**242–251.